

F. Valero · M. Y. Luna · M. L. Martín · A. Morata  
F. González-Rouco

## Coupled modes of large-scale climatic variables and regional precipitation in the western Mediterranean in autumn

Received: 14 August 2002 / Accepted: 20 October 2003 / Published online: 28 January 2004  
© Springer-Verlag 2004

**Abstract** The variability of autumn precipitation in the western Mediterranean and its relationship to the large-scale atmospheric variability during the period 1948 to 1989 is assessed. A singular value decomposition analysis is used to establish modes of coupled variability between regional precipitation and geopotential height (Z300), zonal (U-wind) and meridional (V-wind) wind components at the 300 hPa level. The Z300/precipitation coupling, which accounts for 52% of the total squared covariance, is strong during the autumn. The first Z300 coupled mode, in its positive phase, is characterised by a dipole structure with negative anomalies over Scandinavia and positive anomalies over the Iberian Peninsula in the Z300 and negative precipitation anomalies in the western Mediterranean. In its negative phase, a coupled pattern is found showing a high-over-low block and positive precipitation anomalies over the Mediterranean area. The coupling depicted by the second mode is weaker than that found in the first mode. The second coupled mode (21% of the total squared covariance) is characterised by negative anomalies in the eastern North Atlantic and positive ones over North Africa and the central Mediterranean in the Z300 and negative anomalies in the regional precipitation. Consistent with the results of the two first modes mentioned, the coupled patterns of either U-wind/precipitation or V-wind/precipitation are found to be coherent with those for Z300/precipitation. Composite maps were obtained to give a representation of the average circulation associated with coherent precipitation variability in the western

Mediterranean. The regional impacts of both modes are investigated and the large-scale dynamic patterns presented are important modes of variability. Taking into account data for the whole of the twentieth century, results show that the first singular mode is responsible for the decadal trends and long term changes in precipitation. The late 1970s and 1980s is shown as the drier period and the late 1950s and early 1960s as the wettest years of the century.

### 1 Introduction

Mediterranean climate constitutes an issue of great concern within the context of regional climate variability and climate change studies (IPCC technical summary 2001). Assessment on the potential regional impacts of anthropogenic forcing on Mediterranean climate is necessarily dependent on the available knowledge about natural variability at regional scales and its relationship to the large-scale circulation. Considerable effort has been put into the study of Mediterranean climate variability (Alpert et al. 1990; Bartzokas et al. 1994; Maheras et al. 1999; Maheras and Kutiel 1999; Wibig 1999; Quadrelli et al. 2001; Xoplaki et al. 2003a,b) and of the western Mediterranean area in particular (Corte-Real et al. 1995; Esteban-Parra et al. 1998; Goodess and Palutikof 1998; Trigo and Palutikof 1999, 2001; González-Rouco et al. 2000).

The relationship between western Mediterranean precipitation and large-scale atmospheric circulation patterns has been extensively studied by means of various techniques during the last decades. Several authors have analysed the spatial and temporal variability of the seasonal or annual precipitation over the Iberian Peninsula and its relationship with the North Atlantic circulation patterns and indices by using different multivariate statistical methods (Zorita et al. 1992; Deser and Blackmon 1993; Esteban-Parra et al. 1998; Rodríguez-Puebla et al. 1998). Potential changes in

F. Valero (✉) · A. Morata · F. González-Rouco  
Dpto. Astrofísica y CC. de la Atmósfera, Facultad de CC Físicas,  
Universidad Complutense de Madrid, 28040 Madrid, Spain  
E-mail: valero@fis.ucm.es

M. Y. Luna  
Servicio de Desarrollos Climatológicos,  
Instituto Nacional de Meteorología, Madrid, Spain

M. L. Martín  
Dpto. Matemática Aplicada a la Ingeniería, EITIG,  
Campus de Segovia, Universidad de Valladolid, Spain

Iberian precipitation as a response to increasing atmospheric greenhouse-gas concentrations have also been analysed (von Storch et al. 1993; González-Rouco et al. 2000).

Due to the distinctive orography of Iberia the western Mediterranean climate is confined to a narrow coastal strip of land spanning southwest France, the eastern Iberian coastline and western North Africa. The strip is characterised by an abrupt rise of land from the coast with an area made up of high mountains, which rise to varying heights relatively close to the coastline. This feature fosters rapid use of the very warm, moist air from the Mediterranean Sea over the mountains. This situation favours instability and the release of vast amounts of latent heat. The result is the development of thunderstorms which may be a single supercell or will form a squall line. In particular, the southeast of Spain with annual average precipitation totals as low as 150 mm (Wheeler 1989) constitutes the driest area not only of Iberia but also of Europe and offers a landscape more similar to neighbouring Africa. The western Mediterranean is particularly characterised by floods during the late summer and autumn and dry periods lasting up to several years (Doswell et al. 1998; Romero et al. 2000). The dramatic swings in precipitation constitute one of the dominant forms of climate variability in the eastern Iberian Peninsula. A lot of effort has been made towards the understanding of possible mechanisms for these episodes (Maheras 1988; Corte-Real et al. 1995; Sumner et al. 2001). Several physical and dynamical processes, such as storm track changes, low-level advection of warm, moist air or topographic configuration can play an important role in autumn extreme episodes (Font 2000). At the end of summer and at the beginning of autumn, strong and unstable phenomena show up over both land and sea, because of polar air advection associated with disturbances developing in the proximity of the Mediterranean (Linés 1970). Most of these disturbances usually affect the Mediterranean Iberian coast and the Balearic Islands and cause the heaviest and most important precipitation from September to November. Intensive investigation into the importance of this line of research extends beyond the pure scientific domain since the socioeconomic impacts of such extreme episodes are far from negligible (IPCC Technical Summary 2001). Heat waves and droughts can have disastrous consequences which can affect natural ecosystems and several aspects of societies such as health or economic wealth. Soil degradation causes migration, an issue of particular concern in the southern Mediterranean area. Prolonged droughts, water supply problems and fires can reduce tourism revenues (IPCC policy makers 2001). Thus, advances in understanding the relationships between precipitation anomalies in the western Mediterranean Basin and coherent atmospheric anomaly patterns are extremely relevant to the whole of society.

Previous works on the western Mediterranean have mainly focused on the influence of the North Atlantic

surface climate on the Iberian Peninsula during winter (Zorita et al. 1992; González-Rouco et al. 2000) while less attention has been given to other seasons and other atmospheric levels. The results of these authors suggest that there is a consistent relationship between western Iberian rainfall and climate surface anomalies in the North Atlantic. There are only a few works focused on the winter precipitation variability in the east of the Iberian Peninsula (Lana and Burgeño 1998; González-Hidalgo et al. 2001). Less emphasis has been placed on the relationship between autumn precipitation and large-scale circulation in this area where downscaling models tend to show low predictive skill (Luna et al. 2001; Trigo and Palutikof 2001). Therefore, it is a matter of interest to extend the knowledge of the large-scale circulation patterns which influence the variability of eastern Iberian autumn precipitation.

Although other factors such as sea surface temperature, and land-sea effects can be important in explaining autumn precipitation anomalies, the purpose of this work is to investigate the influence of upper-level large-scale circulation on the precipitation in the western Mediterranean. The present study is aimed at gaining a better insight into the linkage between the western Mediterranean Basin precipitation fluctuations and large-scale circulation anomalies during the autumn season using observational data. The main purpose is to identify and analyse atmospheric circulation patterns related to the precipitation anomalies by means of statistical techniques such as singular value decomposition, composite analysis and correlation analysis (Bretherton et al. 1992; Wallace et al. 1992; Peng and Fyfe 1996). One of the main dynamical large-scale mechanisms for development of precipitating systems along the Mediterranean coast of the Iberian Peninsula is the presence of cut-off lows associated with jet streams and characterised by a strong meridional component (Valero et al. 1997; Esteban-Parra et al. 1998). Baroclinicity and depression development (cyclogenesis) are intimately related to the strength of the 300 hPa flow. The 300 hPa level is therefore selected and the variables used are geopotential height and horizontal wind components.

The organisation of the study is a brief description of the analysis methods and data employed, which is given in Sect. 2. Section 3 is devoted to analysis of the western Mediterranean precipitation variability. The results related to the coupling of the upper-level atmospheric circulation with the precipitation are discussed in Sect. 4. The relationship between precipitation and the low-level atmospheric circulation is described in Sect. 5. Discussion of the main results and conclusions are drawn in Sect. 6.

---

## 2 Methodology and data

The relationship between the large-scale circulation and the precipitation in the western Mediterranean basin is investigated by means of singular value decomposition (SVD) analysis, and briefly here summarised. The present study employs the SVD

methodology described in Bretherton et al. (1992). More details about the SVD analysis can be found in von Storch and Navarra (1995) and von Storch and Zwiers (1999). SVD analysis allows one to find patterns and time series that maximise the fraction of explained covariance between any two fields. Patterns are obtained as the singular vectors of an SVD of the cross-covariance matrix. It will be then sufficient to choose the quantity covariance to measure the agreement between large-scale circulation and the precipitation model.

The SVD analysis can be thought of as a generalisation to rectangular matrices of the diagonalisation of square symmetric matrices, i.e. it is a generalisation of empirical orthogonal functions (EOF) analysis (Lorenz 1956; Davis 1976). Each eigenvalue measures the contribution of each corresponding pair of patterns to the total squared covariance. Each SVD mode consists of a pair of singular vectors, called left and right singular vectors, together with the associated time series, named expansion coefficient time series. The modes are also ordered with respect to their eigenvalues, so that the first pair accounts for the largest squared covariance. The strength of each mode or the strength of the coupling between the two fields is determined by the fraction of the total squared covariance explained by each mode, i.e. the amount of squared covariance fraction (SCF).

The interpretation of the left and right singular vectors is a natural extension of the EOF concept (von Storch and Navarra 1995). If the  $i$ -th singular vector is projected onto a data field, the  $i$ -th expansion coefficient time series for that variable can be obtained. The correlation between the  $i$ -th expansion coefficients of two variables measures the intensity in the relationship between the components of that pair. The heterogeneous correlation pattern for the  $i$ -th left (right) field is defined as the correlation between the left (right) field and the  $i$ -th expansion coefficient for the right (left) field and is proportional to the left (right) singular vector. For display purposes, the time series of expansion coefficients have been normalised by their standard deviation and the corresponding heterogeneous correlation patterns have been multiplied by the data standard deviation so that each SVD spatial pattern represents anomalies.

While the derived modes are statistically constructed, the composite maps represent configurations of the variable that can be compared to observations. Thus, as indications of the relationship between observational patterns and the coupled modes, positive (negative) composites are constructed directly from a number of months with the highest (lowest) expansion coefficients values. They indicate situations in which the corresponding mode is dominant in its positive (negative) phase. The choice of the number of situations is arbitrary and chosen to be 5% of the total number of cases in the dataset, but the resultant total fields give a representation of “average” pattern associated with extreme conditions.

The data employed in this study include geopotential height (Z300) and horizontal wind (U- and V-wind) components at 300 hPa from NCEP Reanalysis (Kalnay et al. 1996). The data are monthly means over a  $2.5^\circ \times 2.5^\circ$  grid for 42-autumns (September–October–November) for the period 1948–1989. The sea level pressure data from the National Center of Atmospheric Research (Trenberth and Paolino 1980) have been used because of the long length of the time series available. These data are monthly means over a  $5^\circ \times 5^\circ$  grid for 91-autumns for the period 1899–1989. For both data sets, the selected domain spans the North Atlantic Ocean, the Mediterranean Sea and Europe from  $20^\circ$  to  $80^\circ\text{N}$ , and from  $100^\circ\text{W}$  to  $40^\circ\text{E}$ . The precipitation data used is a subset of the precipitation dataset for the southwest of Europe described in detail in González-Rouco et al. (2001). This dataset was quality controlled and homogeneity tested therein. This data subset consists of 26 time series (1948–1989) covering the Mediterranean coast of the Iberian Peninsula, south of France and north of Africa (Fig. 1). The list of stations used and their geographical coordinates are shown in Table 1.

Prior to the analysis, all data sets are modified applying a cos (latitude) square root area-weighting to account for the uneven spatial density of the grid. The original data were also detrended and the seasonal cycle was removed by subtracting the long-term

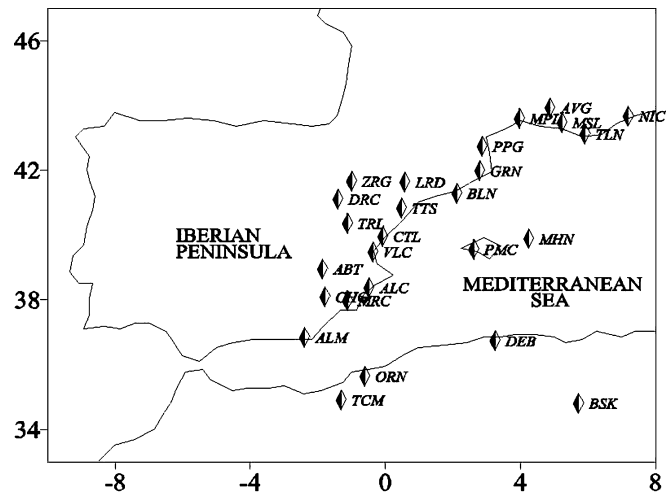


**Fig. 1** Diamonds indicate the precipitation stations for the western Mediterranean Basin. The station codes are shown in Table 1. The  $x$ -axis corresponds to longitude, positive (negative) for degrees east (west). The  $y$ -axis to latitude, positive for degrees north

**Table 1** List of stations used indicating the code for Fig. 1

Code	Name	Latitude (°N)	Longitude (°E)	Altitude (m)
AVG	Avignon	43.92	4.88	24
NIC	Nice	43.67	7.20	5
MPL	Montpellier	43.58	3.97	5
MSL	Marseille	43.45	5.23	6
TLN	Toulon	43.10	5.92	28
PPG	Perpignan	42.73	2.87	43
GRN	Gerona	41.97	2.80	90
ZRG	Zaragoza	41.65	-1.00	240
LRD	Lérida	41.62	0.58	192
BLN	Barcelona	41.28	2.12	420
DRC	Daroca	41.10	-1.40	787
TTS	Tortosa	40.82	0.48	50
TRL	Teruel	40.35	-1.12	900
CTL	Castellón	39.95	-0.07	35
MHN	Mahón	39.88	4.25	82
PMC	Palma de mallorca	39.55	2.62	6
VLC	Valencia	39.47	-0.37	11
ABT	Albacete	38.95	-1.85	704
ALC	Alicante	38.37	-0.48	82
CHG	Cehegín	38.08	-1.78	572
MRC	Murcia	37.97	-1.12	56
ALM	Almería	36.83	-2.38	21
DEB	Dar-el-beida	36.72	3.25	25
ORN	Oran	35.63	-0.60	10
TCM	Tlemcem	34.90	-1.30	80
BSK	Biskra	34.80	5.73	81

mean from each monthly mean to produce monthly anomalies. Finally, standardised anomalies were obtained for all fields. The SVD analysis was then performed on the detrended data to obtain seasonally independent detrended modes. The expansion coefficients are obtained by projecting the original data (i.e. non-detrended) onto the previously derived SVD spatial modes. This allows for a representation of the long-term trends in the time series of expansion coefficients, because the initial detrending of data avoids inflation of the cross-covariance coefficients in the determination of the spatial SVD patterns (Heyen et al. 1996; von Storch and Zwiers 1999; González-Rouco et al. 2001).

### 3 Variability of western Mediterranean precipitation

According to Wheeler (1989) and Font (2000), the western Mediterranean climate is characterised by maxima of precipitation in equinoctial seasons with the absolute maximum in autumn. Mediterranean mean rainfall decreases with latitude except for local anomalies due to local factors. Topographic configurations can be decisive for precipitation records leading to extreme differences between highlands and lowlands or between stations with different exposure to maritime winds (Romero et al. 1998; Font 2000). The patterns of autumn mean precipitation and standard deviation (plotted by a kriging gridding method) can be observed in Fig. 2 for the western Mediterranean area. Given that only two observatories are located on islands, the interpretation of the contours should be made with caution. They must be interpreted as a rough display of the distribution of the parameters related with precipitation. Throughout the study, no comment will be made about land areas without stations. These areas have been whitened as much as possible in order to improve the figures and to mitigate any misinterpretation to the reader. On average, the autumn rainfall amount (Fig. 2a) varies from about 75 mm month<sup>-1</sup> over southern France to less than 35 mm month<sup>-1</sup> over the

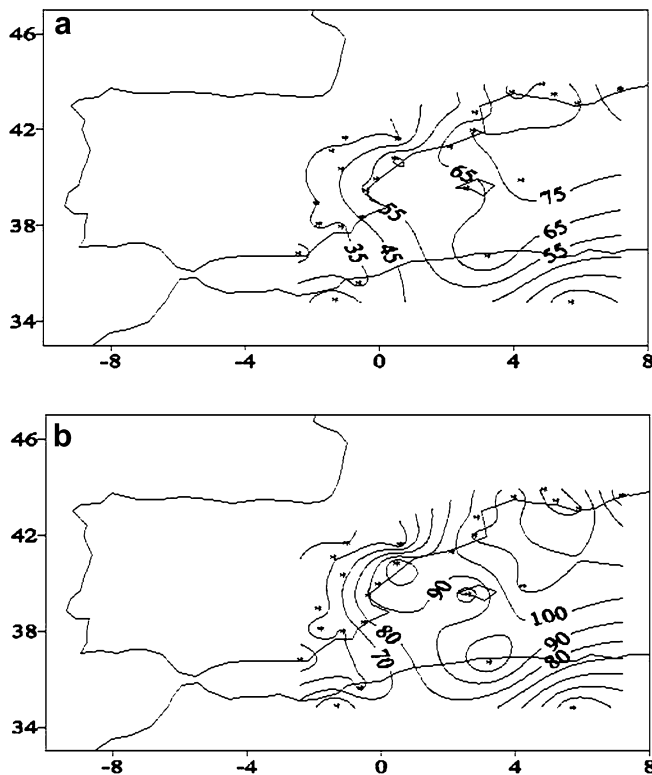


**Fig. 2** a Autumn seasonal mean and b standard deviation of the western Mediterranean Basin precipitation. Contour intervals are 10 mm month<sup>-1</sup>. The position of individual stations is marked by asterisks. The *x*-axis corresponds to longitude, positive (negative) for degrees E (W). The *y*-axis to latitude, positive for degrees N

southern regions. Local maxima are found over Mahon, Tortosa and Dar-el-Beida observatories. Precipitation variability tends to be higher in areas where large rainfall amounts occur, as can be observed in Fig. 2b.

In order to examine the year-to-year fluctuations, a standardised anomaly index (SAI) is constructed by means of temporal (September–November) and spatial averages of the 26 standardised precipitation time series. The SAI evolution (Fig. 3) suggests considerable inter-annual and decadal variability: up to 1955 there are large precipitation fluctuations with two extreme dry autumns and with the wettest autumn of the whole period in 1951 (SAI almost 2 standard deviations); from 1956 to 1964 wet conditions dominate; from 1964 to 1968 precipitation is close to normal; and thereafter large fluctuations appear again. It is noticeable that the two driest years are in the latter period, with 1981 the driest and most anomalous year (SAI just above 2 standard deviations).

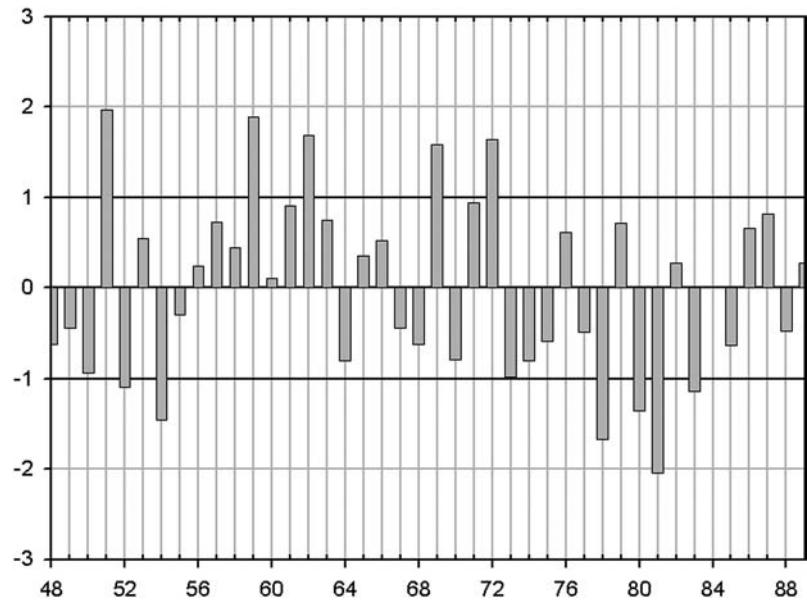
### 4 Coupled patterns between precipitation and upper-level atmospheric circulation

As described in the Introduction, with the objective of identifying the large-scale regimes that are responsible for significantly anomalous precipitation on a monthly scale during autumn, the relationship between western Mediterranean precipitation and large-scale atmospheric circulation is investigated by means of a SVD analysis. The analysis is carried out by diagonalising covariance matrices between the precipitation dataset previously described and either the geopotential height or the zonal or meridional wind components at the 300 hPa level. Table 2 shows the percentage of the SCF explained by each mode and the correlation coefficients between pairs of expansion coefficients for the first five modes of SVD, which give us an idea of the strength of the coupling. In the three analyses, only the two first coupled modes, accounting for more than 70% of accumulated covariance, are considered. The leading coupled modes closely resemble the EOF patterns (not shown) of the corresponding fields, suggesting the existence of recurrent physically coupled modes (Hu 1997). In addition, for the two first modes the correlation values are higher than for the remaining ones. The lower-order modes describe additional circulation-precipitation covariation but may quickly degenerate because of noise (von Storch and Navarra 1995), so for this work just the two first modes are analysed.

#### 4.1 First mode of covariability

The first SVD mode explains 52% of the squared covariance between Z300 and precipitation fields. The first pattern of Z300 anomalies is shown in Fig. 4a. The positive phase of this pattern is characterised by a positive centre of geopotential anomalies over Iberia and a

**Fig. 3** Standardised anomaly index (SAI) for the western Mediterranean Basin precipitation. Units are in standard deviations. The *x-axis* corresponds to time (years)



negative one over Scandinavia and eastern North Atlantic. This configuration is usually associated with the presence of a ridge lying over southwestern Europe at the upper level and a high pressure centre located over Iberia at the surface (as shown in Sect. 5). This atmospheric structure may lead to a deficit of rainfall in the western Mediterranean region. The corresponding coupled precipitation mode (Fig. 4b) shows significant negative weights in the whole area of interest, some shifted east into the Mediterranean.

The negative phase of the Z300 pattern (Fig. 4a with reversed sign) would correspond to a centre of action with strong negative weights over the Iberian Peninsula and a positive centre over the Scandinavian Peninsula. Such a dipole structure result from a blocking pattern. In the region of the block, the weather remains essentially unchanged, as any transient weather disturbances are forced to circumvent the blocking System. Once established, major blocking situations tend to persist for at least a week and appear to represent some quasi-equilibrium state of the atmosphere. Sumner (1954) and Bluestein (1993) named this type of block a “high-over-low” pattern, which occurs most frequently over western Europe. The pattern is also called a split-flow pattern because the basic atmospheric current “splits” around the block. At upper levels, this kind of configuration is usually characterised by a ridge lying over central Europe and Scandinavia and by a trough situated over Iberia. The trough favours meridional incursions of maritime cooler air from the Atlantic Ocean and flows into the western Mediterranean area after rotating around a cut-off low near the Iberian Peninsula. This situation enables precipitation systems to be developed in the western Mediterranean Basin and matches the negative phase of the precipitation pattern shown in Fig. 4b (with reversed sign).

An SVD analysis between horizontal wind at 300 hPa and western Mediterranean precipitation has been also

**Table 2** Squared covariance fraction, SCF, and temporal correlation coefficient, *r*, for the first five modes of SVD analysis corresponding to the three pairs of coupled patterns

<i>k</i>	Z300		U-wind		V-wind	
	SCF (%)	<i>r</i>	SCF (%)	<i>r</i>	SCF (%)	<i>r</i>
1	52	0.64	53	0.67	55	0.64
2	21	0.60	25	0.67	21	0.69
3	11	0.51	7	0.45	12	0.54
4	3	0.45	3	0.51	4	0.49
5	2	0.44	3	0.49	3	0.45

undertaken so that possible imbalances between Z300 and 300 hPa horizontal circulation fields can be determined. Figure 5 shows the first SVD coupled mode between zonal wind and western Mediterranean precipitation. The first mode of U-wind (Fig. 5a) contains a contrasting centre of action over western Europe. There are two negative weight centres which are about equal in value that diverted them away (poleward and equatorward) from the positive centre as a bifurcation of the basic flow of the atmosphere in these latitudes. The opposite phase of the U-wind mode may well then be associated with the split-flow configuration shown in the Z300 field. As the centres of negative anomaly are also centres of maximum wind, it may be concluded that they determine the average position of the polar and subtropical jet stream, respectively. The corresponding pattern of precipitation anomalies (Fig. 5b) depicts similar behaviour to the rainfall configuration shown in Fig. 4b indicating that they respond to the same large-scale atmospheric structure.

Finally, an SVD analysis was also applied to the V-wind component and precipitation fields. Figure 6 displays their respective coupled modes and another dipolar configuration in the heterogeneous pattern develops in this case (Fig. 6a). Here, the pattern consists of a west-east dipole of anomalies with a centre located

**Fig. 4a, b** Heterogeneous patterns of anomalies for the first SVD mode between Z300 and the western Mediterranean precipitation. **a** Z300 (contour interval is 10 gpm) and **b** precipitation patterns (contour interval is 10 mm and zero line omitted). The positive (negative) contours are *solid* (*dashed*). The position of individual stations is marked by *asterisks*. The *x-axis* and *y-axis* as in Fig. 1

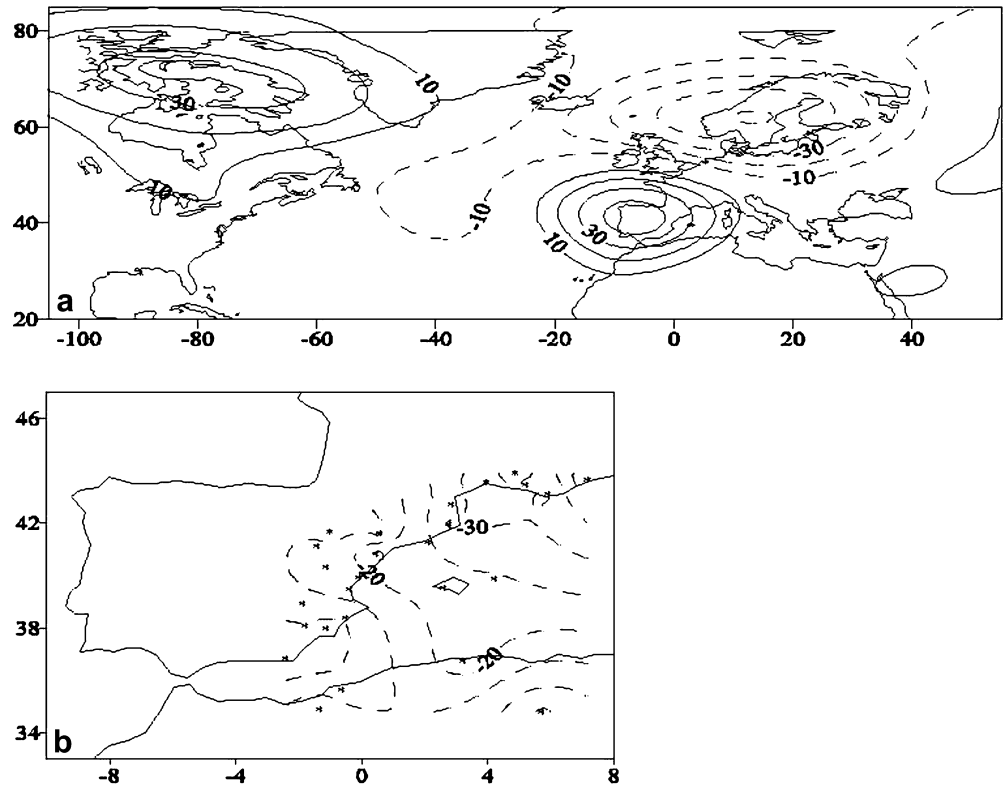
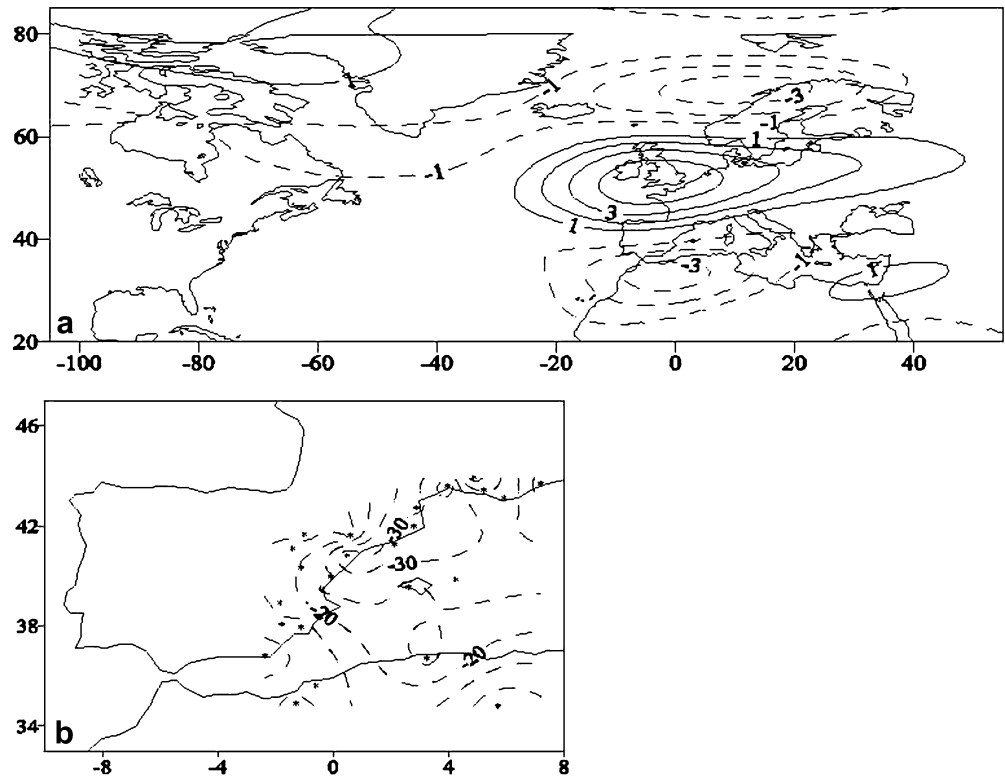


**Fig. 5** Heterogeneous patterns of anomalies for the first SVD between U-wind and the western Mediterranean precipitation: **a** U-wind (contour interval is  $1 \text{ ms}^{-1}$ ) and **b** precipitation patterns (contour interval is 10 mm and zero line omitted). The precipitation contour interval is 10 mm. The positive (negative) contours are *solid* (*dashed*). The position of individual stations is marked by *asterisks*. The *x-axis* and *y-axis* as in Fig. 1



over the east Atlantic and another one over the western Mediterranean Sea. A positive (negative) phase of this pattern, therefore, indicates intensification of both northerly (southerly) winds over the western

Mediterranean and southerly (northerly) wind over the east Atlantic. It can be easily inferred from Fig. 6a that this mode for the V-wind is consistent with a centre of positive geopotential anomalies over Iberia (Fig. 4a)

and with stronger westerlies over Eastern Europe (Fig. 5a). The pattern of precipitation anomalies (Fig. 6b) shows negative values in the whole area according to the dipolar configuration in the V-wind.

In summary, the negative phase of each first mode of the three SVD analyses consistently links a long-lived high-over-low blocking situation to positive precipitation anomalies over the western Mediterranean Basin. Table 3 shows the variances of individual fields explained by the two first significant modes. The precipitation pattern described by the first SVD mode accounts for about 35% of the total precipitation variance and matches the first EOF (not shown) of this variable: the correlation between the SVD expansion coefficient time series and the first principal component is 0.96. The Z300, U-wind and V-wind patterns described by the first SVD explain 11%, 8% and 12% of their respective variance. These large-scale patterns agree well with the corresponding second EOF: correlations between the Z300, V-wind and U-wind first expansion coefficient time series and second principal components are 0.77, 0.51 and 0.86, respectively, significant at the 0.01 level.

The expansion coefficient time series associated with the first mode are shown in Fig. 7a–c. In general, there is

a similar time evolution in all cases. The correlation values between the pairs of time series are 0.64, 0.67 and 0.64 (Table 2), significant at the 0.01 level. These moderately high correlation values point to the high degree of coupling between the large-scale variables and regional precipitation. Moreover, a similar pattern of variability in regional precipitation is produced by the first SVD mode regardless of the large-scale variable considered (Z300, U-wind or V-wind) indicating that the same dynamic atmospheric structure is represented by that mode. The correlation absolute value between any of the precipitation expansion coefficient time series (Fig. 7) and the spatial average of precipitation in Fig. 3 is higher than 0.9 indicating that the first SVD mode is responsible for the decadal trends and long-term variability of precipitation in the western Mediterranean Basin. Thus, the low precipitation values observed in Fig. 3 since the beginning of the 1970s could be related to an apparent rising trend in the large-scale variables expansion coefficients. In fact, a Mann-Kendall test (Goossens and Berger 1986) has been applied to the time series of Figs. 3 and 7 and the rising trend result is statistically significant at the 0.1 level. This positive trend indicates that the patterns in Figs. 4a, 5a and 6a tend to

**Fig. 6** Heterogeneous patterns of anomalies for the first SVD between V-wind and the western Mediterranean precipitation: **a** V-wind (contour interval is  $1 \text{ ms}^{-1}$ ) and **b** precipitation patterns (contour interval is 10 mm and zero line omitted). The positive (negative) contours are *solid* (*dashed*). The position of individual stations is marked by *asterisks*. The *x*-axis and *y*-axis as in Fig. 1

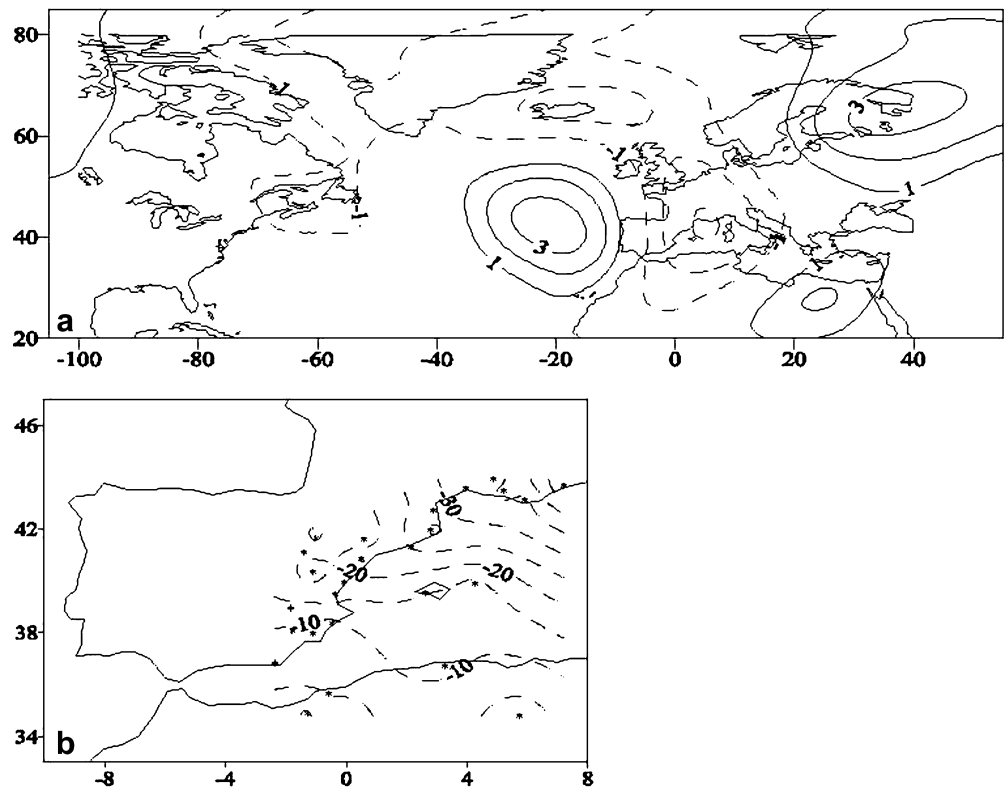


**Table 3** Variance of individual fields explained by the two first modes of the three SVD analyses. The variance is in percent

<i>K</i>	Z300 variance	Precipitation variance	U-wind variance	Precipitation variance	V-wind variance	Precipitation variance
1	11	35	8	35	12	34
2	12	14	12	12	9	15

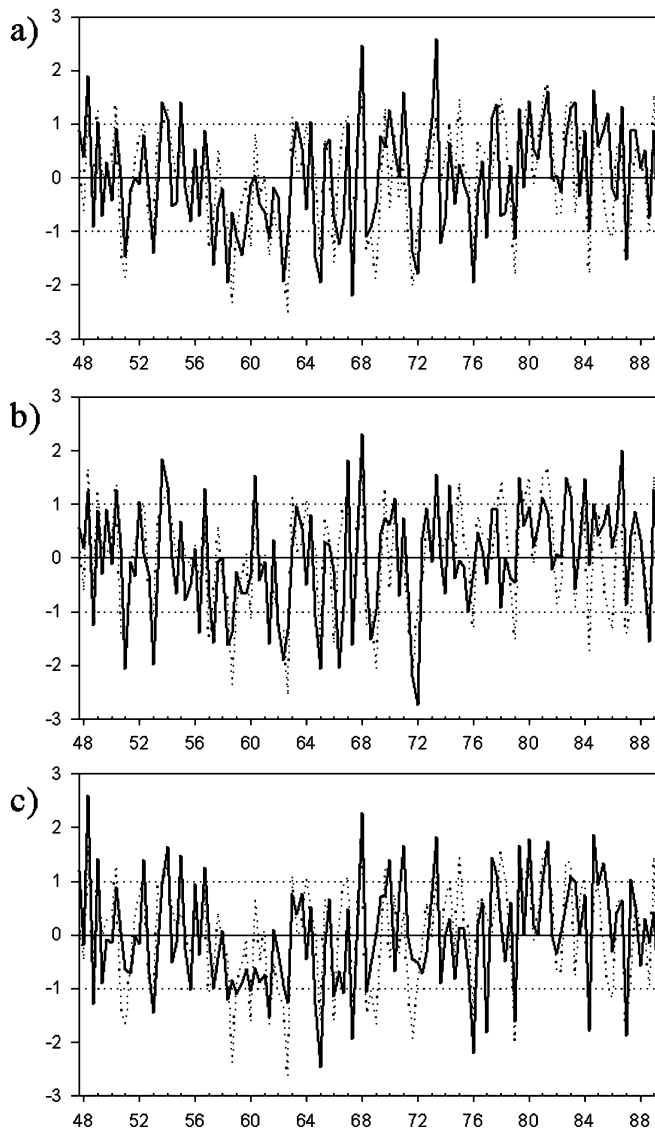


**Fig. 7** The expansion coefficient time series of the first SVD mode: **a** Z300/precipitation; **b** U-wind/precipitation; **c** V-wind/precipitation. Units are in standard deviations. The *x*-axis corresponds to time (years). In each panel, the *solid curves* correspond to the expansion coefficient time series of the respective large-scale fields and the *dashed curves* to that of the precipitation

persist in their positive phase. Consequently, the fact that negative values of large-scale variables expansion coefficients have been less frequent since the 1970s indicates that the high-over-low blocking situation has been less prevalent. After applying a spectral analysis (Jenkins and Watts 1968) to the time series of Fig. 7, no significant concentration of variance is found in any frequency. Further comments on the decadal variability and trends for the last century will be made in Sect. 5.

#### 4.2 Second mode of covariability

The second SVD mode explains 21% of the squared covariance between Z300 and precipitation fields.

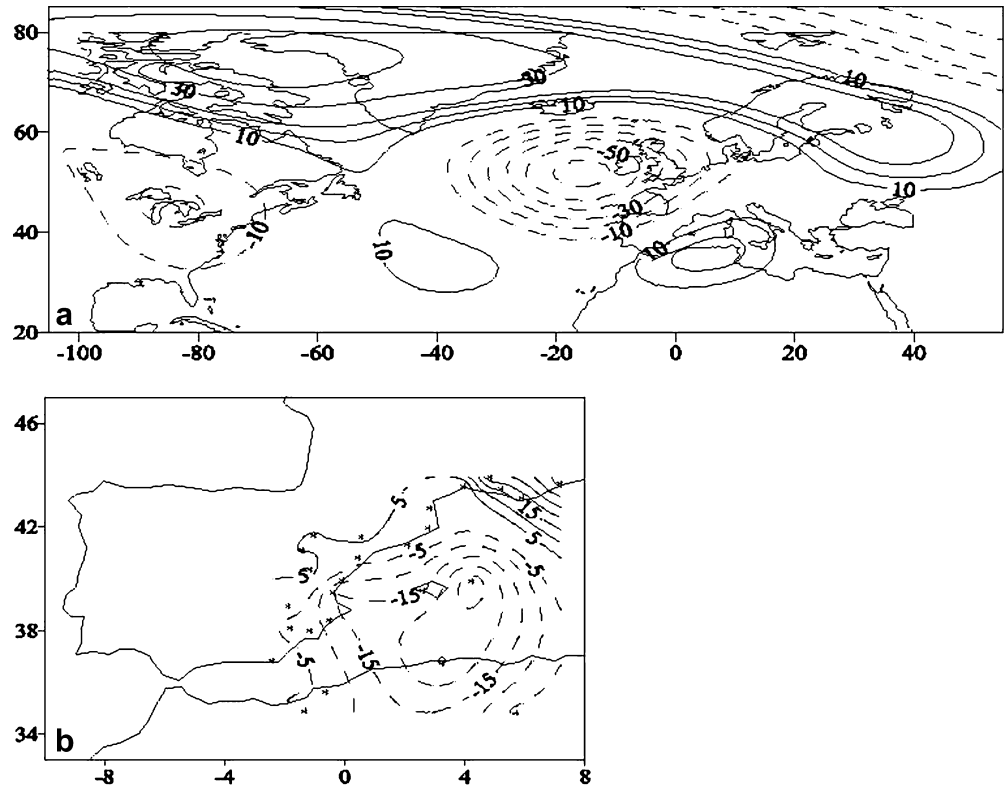
Figure 8a displays the second Z300 mode in its positive phase with a centre of negative anomalies to the west of the British Isles and a centre of positive anomalies over western North Africa and the central Mediterranean. We may notice that this pattern conveys a southwesterly air flow towards Iberia. This situation results in covariation with the precipitation anomalies pattern displayed in Fig. 8b and gives rise to positive precipitation anomalies over northeast Iberia and southeast France and negative ones over southeast Iberia, North Africa and Balearic Islands. In the opposite phase of this mode, positive anomalies are situated over the eastern North Atlantic and negative ones over the southwestern Mediterranean Sea, which are associated with positive precipitation anomalies.

Figure 9 provides the second mode between the U-wind component and western Mediterranean precipitation. The mentioned southwesterly advection over Iberia is indeed found in Fig. 9a for the U-wind pattern. An area of positive anomalies centred at about 40°N latitude over the Iberian Peninsula and two negative centres are found to the northwest of Great Britain and south of the Atlas Mountains. We may notice that the corresponding precipitation pattern (Fig. 9b) is really much the same as that outlined in Fig. 8b. The spatial correlation between both patterns is very high with a value of  $r = 0.97$ . The opposite phase of this mode suggests a subtropical link between atmospheric circulation and western Mediterranean precipitation. This link is made clear by the existence of a positive centre of zonal wind anomalies, situated at about 30°N latitude, associated with positive precipitation anomalies in southeastern Iberia, western North Africa and the Balearic Islands.

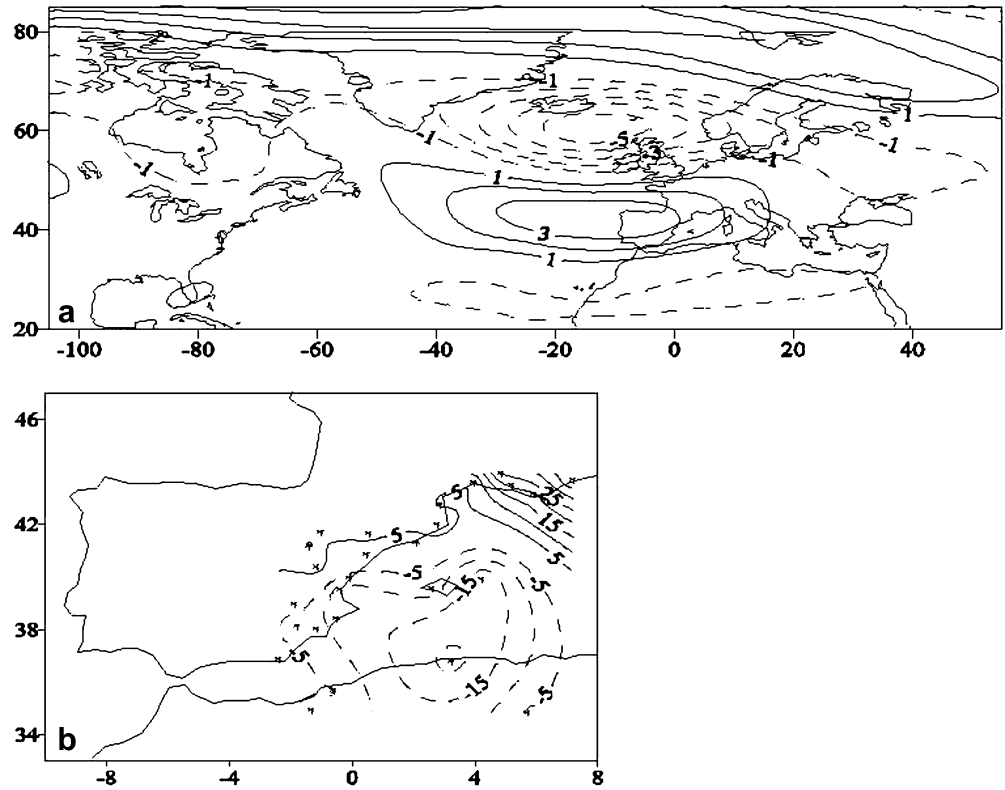
The results of the SVD analysis applied to the V-wind component and precipitation fields are shown in Fig. 10. Figure 10a presents the second V-wind mode and contains a west-east dipolar configuration. The positive anomalies are situated over eastern Europe and the negative ones over the central Mediterranean Sea. The positive phase of this pattern is related with to reinforcement of southerlies over western Europe in agreement with the anomalous SW advection over Iberia described for the Z300 pattern and is responsible for the dry conditions over the south of the western Mediterranean Basin. Figure 10b clearly shows that the pattern of precipitation anomalies matches the one displayed in Figs. 8b and 9b. The spatial correlation values between the anomalies displayed in Fig. 10b and the one displayed in Figs. 8b and 9b are 0.90 and 0.86, respectively. The negative phase instead indicates that wet conditions over southeastern Iberia, western North Africa and the Balearic Islands are associated with intensifying southerlies over the central Mediterranean. This situation is in good agreement with the negative phase of the corresponding Z300 pattern.

The second coupled precipitation mode accounts for more than 12% of the total precipitation variability and its main feature is that it determines two different zones

**Fig. 8 a, b** Same as Fig. 4 except for the second SVD mode. Contour interval in precipitation patterns is 5 mm



**Fig. 9 a, b** Same as Fig. 5 except for the second SVD mode. Contour interval in precipitation patterns is 5 mm



of precipitation behaviour: a northern zone related to extratropical atmospheric circulations and a southern zone associated with subtropical atmospheric

circulations. This mode therefore separates the influence of extratropical and subtropical atmospheric circulation for the western Mediterranean precipitation.

**Fig. 10 a, b** Same as Fig. 6 except for the second SVD mode. Contour interval in precipitation patterns is 5 mm

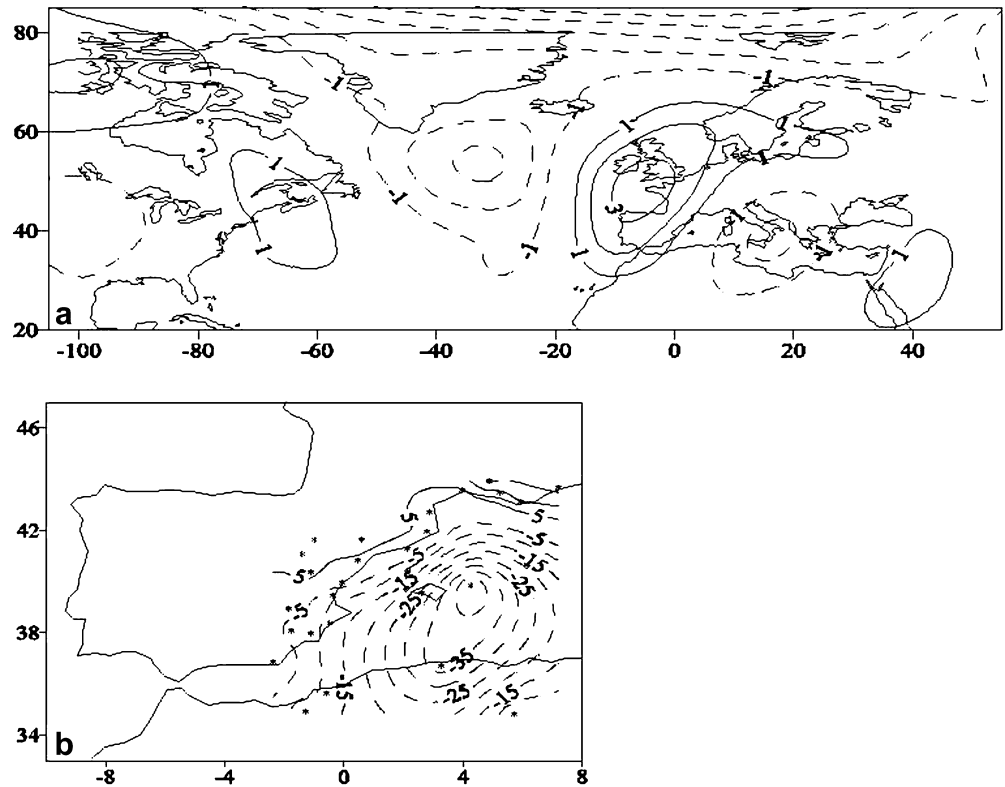


Figure 11 depicts the expansion coefficient time series of the second SVD mode. In general, the Z300, U-wind and V-wind time series exhibit consistent fluctuations with their corresponding precipitation series. The significant correlation values between the pairs of time series are 0.60, 0.67 and 0.69, respectively, and indicate a notable association between them (Table 2). Neither significant variability is concentrated at any frequency after applying a spectral analysis of the time series nor are significant trends found after applying the Mann-Kendall test.

## 5 Relationship between precipitation and large-scale atmospheric circulation

In order to gain more insight into the coupling between the western Mediterranean precipitation and both upper-level and surface circulation, simultaneous correlations between SLP at each grid point and the expansion coefficient time series of either the first or the second mode are computed. Figure 12 shows the correlation maps between the SLP field and either Z300 or the precipitation coefficient series for the two modes. Correlation values higher than 0.17 in absolute value are significant at the 0.05 level by means of a non-parametric test V-wind component for the Spearman correlation coefficient where this significance is calculated without reference to correlations between grid points. The SLP patterns associated with the Z300 time series for the two modes (Fig. 12a, b) and those associated

with the corresponding precipitation time series (Fig. 12c, d) are very similar. For the first SVD mode, both Z300 and precipitation correlation maps (Figs. 12a and c) depict a double dipole over the entire domain, specially in the Z300 map. Aside from the left dipole, a negative zone extending from the central Atlantic to Scandinavia and a positive zone centred over North Africa can be noticed. An examination of this configuration and the corresponding Z300 pattern in Fig. 4a suggests that both surface and upper-level circulation are linked to the precipitation correlation field shown in Fig. 4b. Figure 12b and d shows correlation maps between SLP field and either Z300 or the precipitation coefficient series of the second mode. In both figures, an centre of action (with negative values in these maps) off the north coast of the Iberian Peninsula, with a large area of outstanding correlation, dominates the western European coastline.

To examine the circulation features associated with the described correlation patterns, positive (negative) composites of the distribution of Z300 (with wind vectors superimposed on it) SLP and precipitation anomalies are built up from the 5% highest (lowest) expansion coefficients. The positive composite maps for the first mode (Fig. 13a–c). Figure 13a shows a weak trough located over Scandinavia and a pronounced ridge lying over southwestern Europe. The lack of wind vectors over the western Mediterranean region is in good agreement with the Z300 field. Figure 13b displays the positive composite map for the SLP field. A high pressure zone extends from the western Atlantic into the

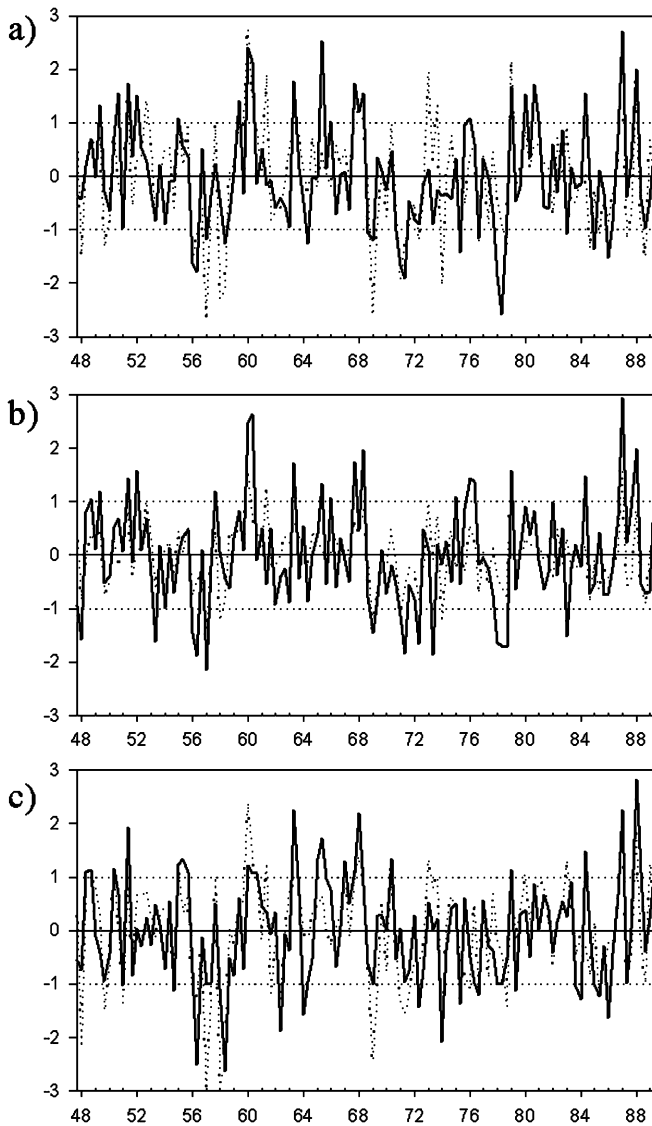


Fig. 11 a–c Same as Fig. 7 except for the second SVD mode

eastern Mediterranean and a low pressure area is found east of Scandinavia. These upper and surface configurations bring below-normal precipitation over the western Mediterranean area as noted in the precipitation composite map shown in Fig. 13c. Alternatively, negative composites of Z300, wind vector, SLP and precipitation are shown in Fig. 14. The Z300 field (Fig. 14a) is characterised by a split flow over western Europe. At 300 hPa, the ridge lying over central Europe and Scandinavia and the eastward tilted trough situated over SW Iberia and the Canary Islands favour advection of Atlantic air towards the western Mediterranean. The SLP composite field (Fig. 14b) shows a *col* (Bluestein 1992) over the Iberian Peninsula. The *col* (common in the “horse latitudes”) is the intersecting zone between an anticyclonic axis (joining two high pressure centres facing each other) and a cyclonic axis (joining two low pressure centres facing each other). A *col* is characterised by substantial deformation in their vicinity and

consequently is highly related to vorticity and instability. Valero et al. (1997) have shown that these large-scale physical and dynamical configurations are related to extreme rainfall episodes in the western Mediterranean. In fact, Fig. 14c shows how the high precipitation anomalies are associated with the split-flow/col pattern.

For the second mode, the positive composite maps of Z300 with wind vector superimposed, the SLP and the precipitation anomaly are shown in Fig. 15. At the upper-level (Fig. 15a), ridge is found at subtropical latitudes and a noticeable trough is situated over the British Isles forcing an increase in zonal wind at 40°N latitude and therefore in maritime humid air over Iberia. The low over the British Isles (Fig. 15b) advects western maritime air over the Iberian Peninsula. This atmospheric structure is usually responsible for rainfall over the whole of Iberia with lower values to the south of the western Mediterranean Basin (Linés 1970; Font 2000). Figure 15c shows that above-normal precipitation prevails over northwestern Iberia and negative anomalies are situated over southeastern Iberia. Figure 16 corresponds to the composite data for the Z300, wind, SLP fields and precipitation anomalies obtained from the negative phase of the second mode. Figure 16a shows a ridge situated northward of the Azores Islands, a retrogressive trough over the western Mediterranean and a subtropical jet stream over North Africa. The composite map also shows intrusion of northern (cool) air. This configuration favours cyclonic horizontal wind shear and unstable conditions over the western Mediterranean. Figure 16b shows no apparent signal associated with the upper-level trough, the main surface characteristic being a high to the north of the Azores Islands with some NE advection of wet, warm air flow over the Spanish Mediterranean coast. According to Valero et al. (1997), lower level warm advection and cold advection aloft, juxtaposed with the cyclonic vorticity on the left side of the jet stream exit region, merge to drive large-scale instability conditions that result in above-normal precipitation over the southwestern Mediterranean region (Fig. 16c).

### 5.1 Spatial and temporal context

The analysis presented has a marked regional character since it focuses on the western Mediterranean coastal precipitation. The regional patterns of precipitation anomalies obtained from the SVD analysis in the previous sections are likely to be part of a broader spatial response of precipitation to the SVD large-scale anomaly configurations presented in Figs. 4–6 and 8–10. In order to gain spatial perspective into the precipitation response to the dynamics possibly associated with the derived patterns, field correlation maps are shown in (Fig. 17) between the NCEP (Kalnay et al. 1996) precipitation dataset and the precipitation expansion coefficient time series corresponding to the first and second SVD modes between 1948 to 1989. For both cases, the

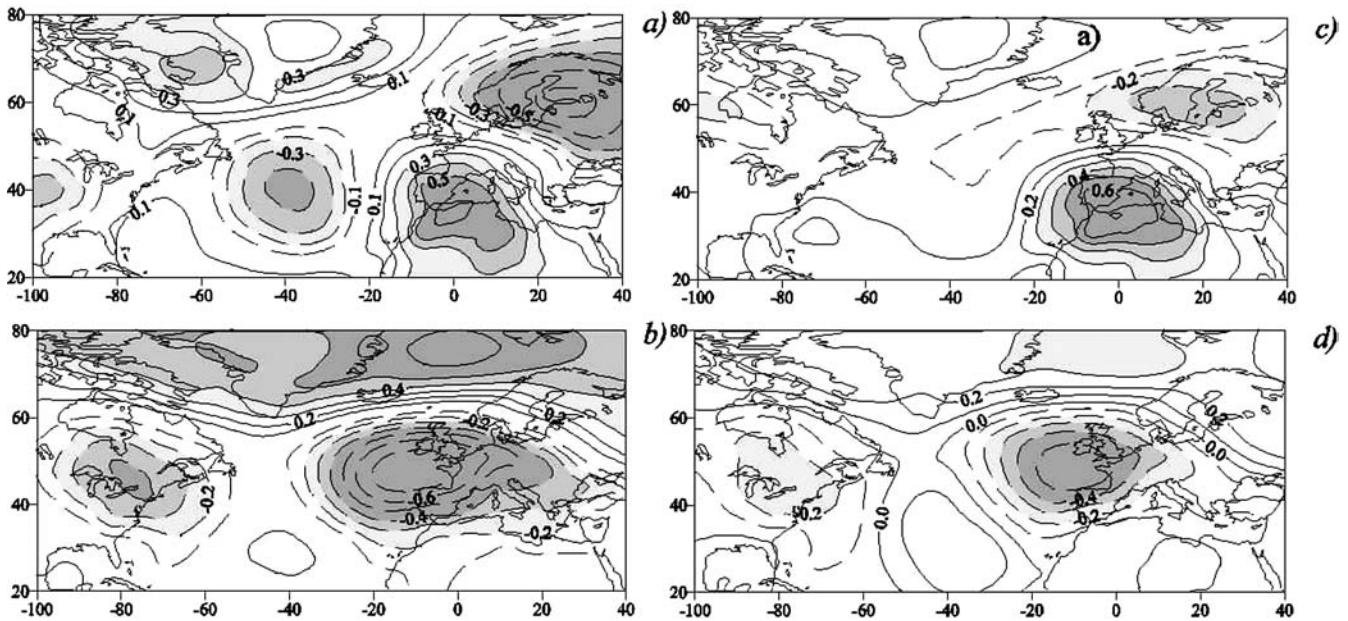


**Fig. 12** Patterns of correlation coefficients between SLP and **a** Z300 first mode time series; **b** Z300 second mode time series; **c** precipitation first mode time series; **d** precipitation second mode

time series. Positive (negative) contours are *solid (dashed)*. Significant correlation areas at the 0.05 level are *shaded*. The *x-axis* and *y-axis* as in Fig. 1

precipitation time series corresponding to the Z300 case were chosen. Each correlation pattern agrees well over the east of the Iberian Peninsula with the corresponding precipitation anomalies. For the first mode, the correlation pattern shows negative anomalies over the whole of the Iberian Peninsula and those of opposite sign over northern Europe. This dipole pattern is in good agreement with the split-flow pattern discussed before. For the second mode, the chart of the correlation coefficients shows an area of negative values over the northwestern African coast reaching the east of the Iberian Peninsula, which gives way to positive correlation values over northeastern Iberia and southern France. The area of positive correlation values extends to the west and north covering most of western Europe. In addition, it can be pointed out that the areas of positive (negative) correlation in Fig. 17 coincide with the areas of negative (positive) geopotential anomalies in the Z300 SVD patterns in Figs. 4 and 8. Figure 17 enlarges the spatial perspective of the anomaly patterns. The results are robust since essentially the same patterns of correlation are obtained (not shown here) when performing the analysis with an independent precipitation dataset like the gridded 5x5 latxlon version of the Global Historical Climatology Network (Eischeid et al. 1995)

The correlation patterns in Fig. 17 suggest that the temporal variations of both SVD modes described may have a spatial impact on precipitation that goes beyond the limited area of the western Mediterranean coasts. For instance, Fig. 17a shows that the first mode may contribute not only to the decay of precipitation in the western Mediterranean since the 1970s, but also to an increase of precipitation over Scotland and the whole Baltic Sea. In order to check this point the spatial

window (52.4–61.8)°N × (11.25–24.4)°E, covering most of the Baltic Sea area, was selected from the NCEP precipitation data for the SON months of the period 1948 to 1989. The correlation between the average precipitation anomalies for this box and the spatial average of the 26 precipitation time series used here is –0.46 (significant at the 0.05 level).

One remark is necessary on the use and reliability of the NCEP precipitation data. While the extension and large-scale features of the maps in Fig. 17 can be considered realistic, the values of correlation on the local scales should be taken with caution since the simulated precipitation suffers from limitations of the sub-grid scale parametrisations and the coarse resolution and topography of the model employed in the reanalysis (Kalnay et al. 1996). The reliability of the NCEP precipitation on the large scale can be attributed to the realistic simulation of the midlatitude cyclones (Janowiak et al. 1998; Widmann and Bretherton 2000). The reason for choosing this dataset is that the NCEP offers a spatially homogeneous representation over land and ocean through the whole period of analysis (1948 to 1989) which is not provided by other precipitation datasets (Eischeid et al. 1995; New et al. 1999, 2000)

Figure 3 showed that while the late 1970s and early 1980s were drier in the western Mediterranean, the late 1950s and early 1960s were wetter, a feature supported by the first mode (Fig. 7). On the other hand, Fig. 18 helps to put the period 1948 to 1989 into the perspective of the long term variability in the twentieth century. The spatial average for the 26 time series used in this study (MEAN) is shown, indicating that actually the late 1970s and early 1980s were the driest years in the whole century and the 1960s the wettest. Highlights are also a

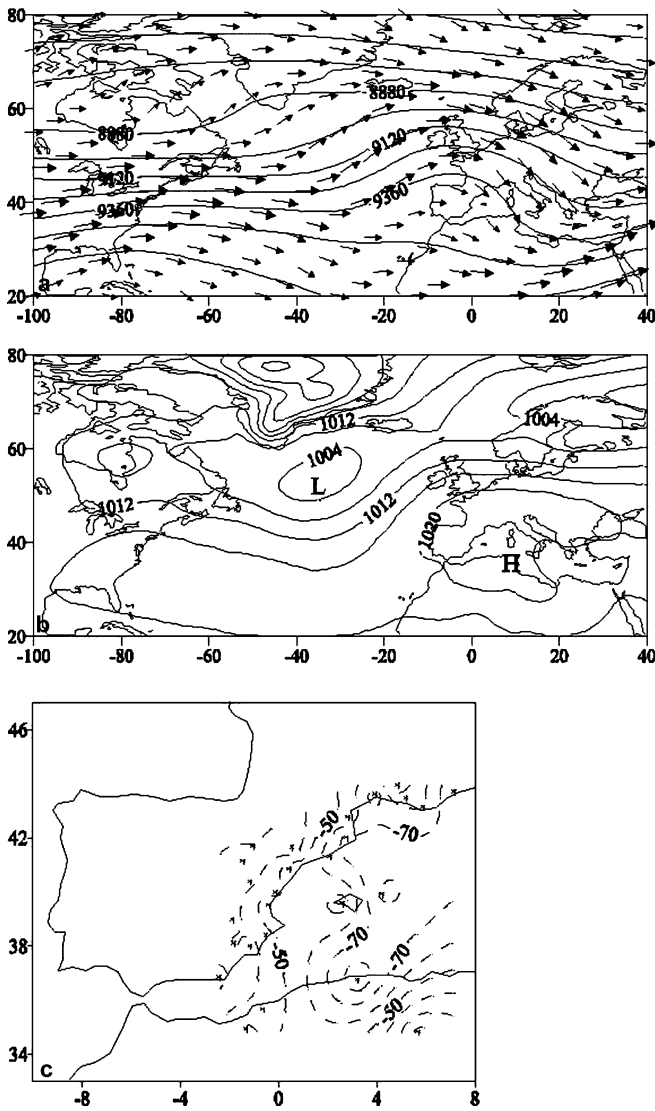


Fig. 13 Positive composite maps of the first mode: a Z300 (gpm) with wind vectors superimposed ( $\text{ms}^{-1}$ ); b SLP (hPa) and c anomalies of precipitation (mm) with station positions marked by asterisks. The x-axis and y-axis as in Fig. 1

dry period in the 1940s and short wet periods close to 1910 and 1920. If the whole twentieth century is considered, a negative trend of  $-1 \text{ mm/decade}$  arises (significant at the 0.1 level).

The good correlations between the large-scale expansion coefficient time series and those of precipitation for the first mode (Fig. 7) indicate that the large-scale dynamics is responsible for those wet and dry periods, at least since 1948. Further insight into this relationship can be gained if the whole century is taken into account. This can be done with the NCAR SLP dataset (Trenberth and Paolino 1980), the only large-scale atmospheric variable which spans the whole century. An SVD analysis comparable to the previous ones presented herein was done between the SLP and the precipitation dataset for the period 1948 to 1989. Results compare well with those presented for Z300 and the

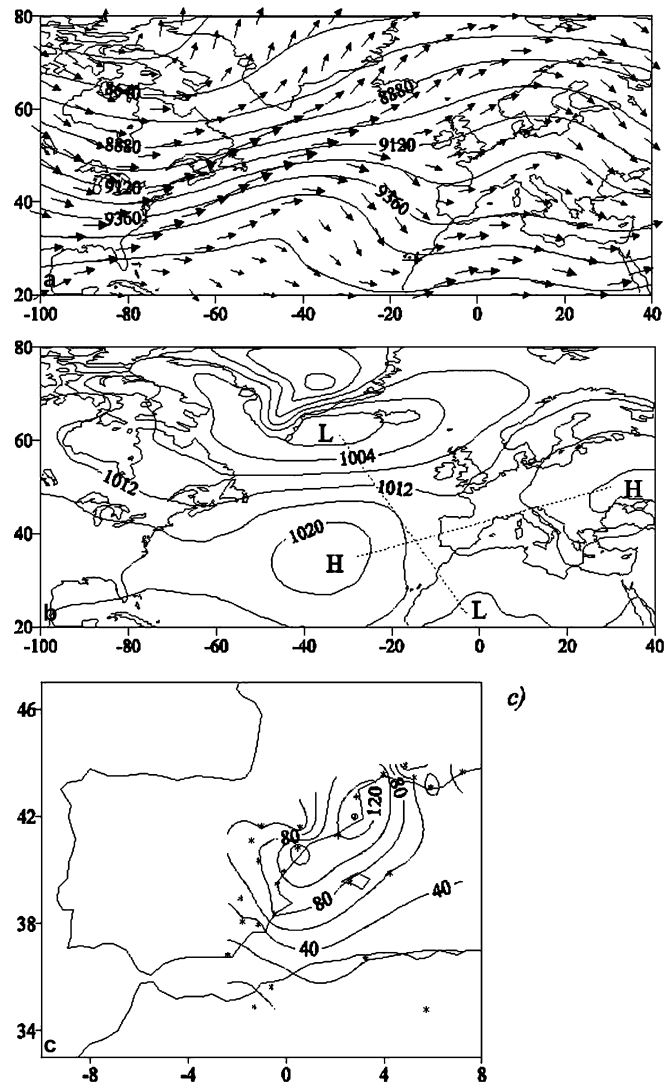


Fig. 14 a–c Same as Fig. 13 except for negative composite maps. Ridge axis and trough axis marked by dashed line

U-wind and V-wind components: the correlation between the SLP and precipitation expansion coefficient time series amounts to 0.66, which is significant at the 99% confidence level. The resulting SLP positive and negative composites (not shown) are on a par with those presented in Figs. 13b and 14b. Figure 18 also shows the projection (von Storch and Zwiers 1999) of the original SLP and precipitation fields for the period 1900 to 1989 onto the SVD corresponding patterns. The resulting time series are highlighted with the acronyms SLP and PREC in Fig. 18. Both time series agree fairly well with correlations of 0.83 and 0.96 between the corresponding coefficient expansion time series for the period 1948 to 1989, respectively. It is noticeable that this centenary time series is very similar to those of the first mode in Fig. 7 and has turned out to be the pattern that best matches the observed precipitation variability. The correlation coefficient between SLP and PREC is 0.61 (significant at the 95% level) for the period 1900 to 1989.

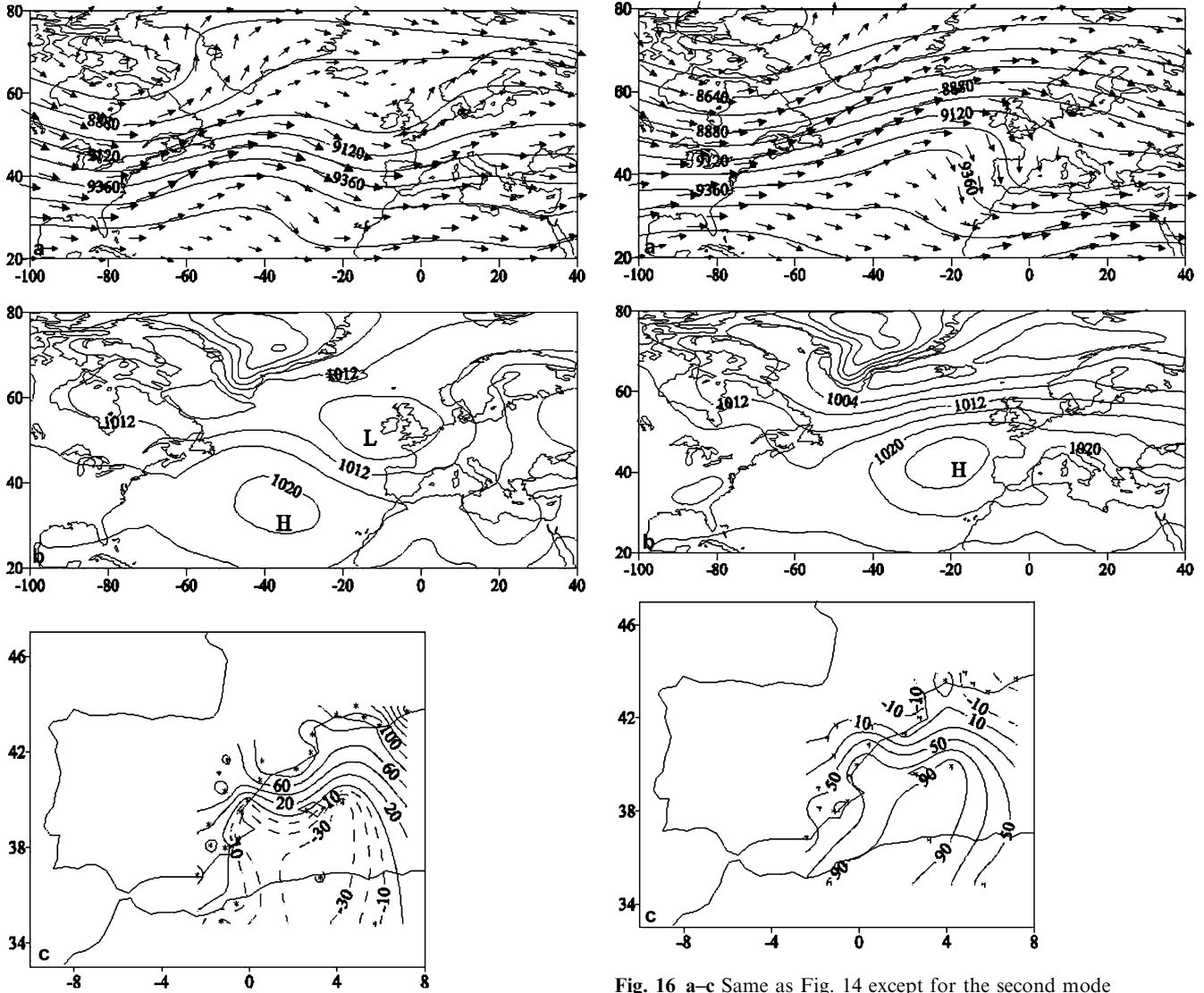


Fig. 15 a–c Same as Fig. 13 except for the second mode

Fig. 16 a–c Same as Fig. 14 except for the second mode

These results suggest that long-term evolution of the large scale variable corresponding to the first coupled SLP and PREC mode are related through the whole period of analysis (1900 to 1989). Furthermore, it is plausible that the lower troposphere SLP configurations of Figs. 13b and 14b hold their relationship for the first half of the twentieth century with the high tropospheric fields described in Figs. 13a and 14a as well. Therefore it is argued that the positive and negative phases of the modes described in Sect. 4.1 are likely to be responsible for the climate variability of western Mediterranean precipitation (Fig. 18) through the twentieth century.

## 6 Discussion and conclusion

The covariability of autumn precipitation over the western Mediterranean and large-scale upper atmospheric circulation has been examined by means of SVD

analysis. In order to characterise the atmospheric circulation, 300-hPa geopotential height and horizontal wind components of 42 autumns (SON) from 1948 to 1989 have been used. For the same period, 26 precipitation time series covering eastern Iberia, southern France and western North Africa have been considered. The two leading modes of the SVD analysis explain over 70% of the total covariability between the atmospheric variables and the western Mediterranean precipitation and almost 50% of the precipitation variability itself, a far from negligible amount. The remaining 50% is likely to be due to other factors but their study would require another kind of approach, possibly with daily data and another methodology.

The first mode (Figs. 4–6) indicates that above-normal precipitation values are determined by the presence of a closed circulation system aloft determined by a high-over-low blocking geopotential height pattern characterised by split-flow around a high located over northern Europe and Scandinavia and a low situated

**Fig. 17** Field correlation maps between the precipitation expansion coefficient time series and the NCEP reanalysis precipitation dataset for the period 1948 to 1989: **a** first mode using the precipitation SVD time series in Fig. 7b and **b** second mode using the precipitation SVD time series in Fig. 11b. Significant correlation areas at the 0.05 level are shaded. The x-axis and y-axis as in Fig. 1

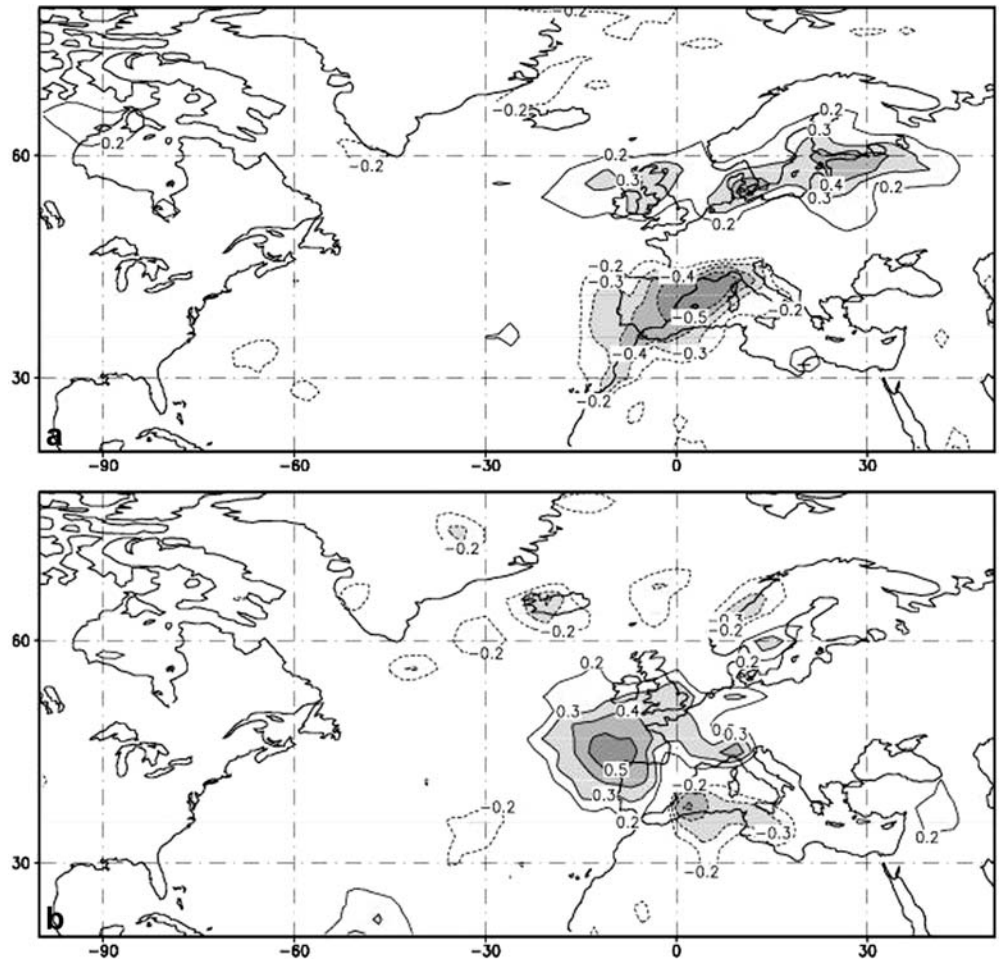
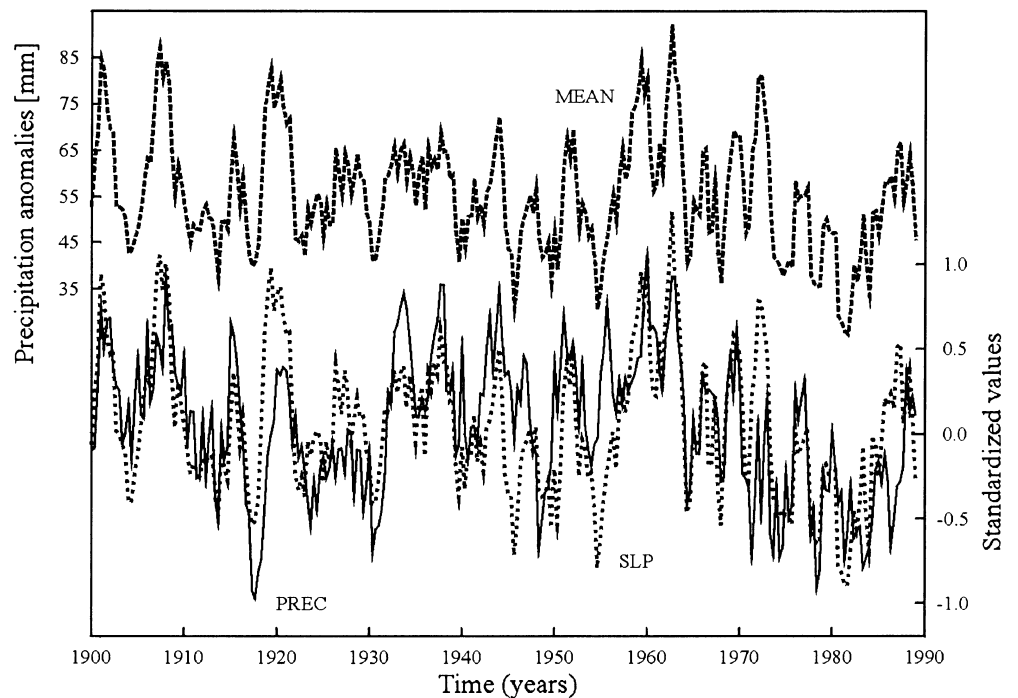


**Fig. 18** *Top*: spatial average (*MEAN*) of the 26 time series of precipitation (September to November values) for the period 1900 to 1989. *Bottom*: projections of the *SLP* and precipitation (*PREC*) datasets for the period 1899 to 1989 onto the corresponding patterns obtained as the first mode in an SVD analysis for the period 1948 to 1989. All time series are 2-year low pass moving average filters



over Iberia. In the blocking region the weather remains essentially unchanged, as any transient weather disturbances are forced to circumvent the block. The SVD patterns of the zonal and meridional wind components are dynamically coherent with the geopotential height configuration and indicates that the first mode of the three SVD analyses represents a well-defined large-scale atmospheric structure.

The second mode (Figs. 8–10) establishes a separation in the response of western Mediterranean precipitation to extratropical and subtropical atmospheric circulations. While above-normal precipitation in the northern area is associated with negative geopotential height anomalies over eastern North Atlantic and anomalous westerlies at 40°N latitude, in the southern area positive precipitation anomalies are related to negative geopotential height anomalies over western North Africa and reinforced westerlies at 30°N latitude.

The regional impacts of both SVD modes also reach the southwest of Europe and the Baltic regions in the case of the first SVD mode and western Europe in the case of the second SVD mode (Fig. 17). Therefore, it should be expected that the large-scale dynamic configurations presented in this study arise as important modes of variability if regional precipitation is assessed in any of the mentioned regions.

An analysis of the SLP and precipitation through the 1900 to 1989 period yields the result that the first SVD mode is responsible for the decadal and long term changes in precipitation through the twentieth century (Fig. 18). Thus, a last comment can be made about the relevance of these results in climate variability and climate change studies. Transient climate simulations with global general circulation models provide an ideal framework in which the long term evolution of large-scale atmospheric patterns can be studied (von Storch et al. 1993; González-Rouco et al. 2000) both in climate simulations of future anthropogenic scenarios (IPCC technical summary 2001) and in paleoclimate simulations including the estimated historical evolution of external forcing (Cubasch et al. 1997). Assessment of the behaviour of large-scale patterns can provide information for the evolution of precipitation in scales below that of the resolution of the climate models, a problem of relevance to downscaling applications.

**Acknowledgements** NCEP Reanalysis data were provided by the NOAA-CIRES Climate Diagnostics Center, Boulder, Colorado, USA from their Web site at <http://www.cdc.noaa.gov>. The authors would like to thank the anonymous reviewers for their helpful comments which have contributed to improving this study. This work has been supported by the research project REN2000-0786.

## References

- Alpert P, Neeman BU, Shay-El Y (1990) Climatological analysis of Mediterranean cyclones using ECMWF data. *Tellus* 42A: 65–77
- Bartzokas A, Metaxas DA, Ganas IS (1994) Spatial and temporal sea-surface temperature covariances in the Mediterranean. *Int J Climatol* 14: 201–213
- Bluestein HB (1992) Synoptic dynamic meteorology in midlatitudes. Vol. I. Principles of kinematics and dynamics. Oxford University Press, Oxford, UK, pp 431
- Bluestein HB (1993) Synoptic dynamic meteorology in midlatitudes. Vol. II. Observations and Theory of Weather Systems. Oxford University Press, Oxford, UK, pp 594
- Bretherton CS, Smith C, Wallace JM (1992) An intercomparison of methods for finding coupled patterns in climate data. *J Clim* 5: 541–560
- Corte-Real J, Zhang X, Wang X (1995) Large-scale circulation regimes and surface climatic anomalies over the Mediterranean. *Int J Climatol* 15: 1135–1150
- Cubasch U, Voss R, Hegerl G, Waskewitz J, Crowley TJ (1997) Simulation of the influence of solar radiation variations on the global climate with an ocean–atmosphere general circulation model. *Clim Dyn* 13: 757–767
- Davis R (1976) Predictability of sea surface temperature and SLP anomalies over the Northern Hemisphere. *J Phys Oceanogr* 6: 249–266
- Deser C, Blackmon ML (1993) Surface climate variations over the North Atlantic ocean during winter: 1900–1989. *J Clim* 6: 1743–1753
- Doswell III CA, Ramis C, Romero R, Alonso S (1998) A diagnostic study of three heavy precipitation episodes in the western Mediterranean Region. *Weather Forecast* 13: 102–124
- Eischeid JK, Baker CB, Karl TR, Diaz HF (1995) The quality control of long term climatological data using objective data analysis. *J Appl Meteorol* 34: 2784–2804
- Esteban-Parra MJ, Rodrigo FS, Castro-Diez Y (1998) Spatial and temporal patterns of precipitation in Spain for the period 1880–1992. *Int J Climatol* 18: 1557–1574
- Font I (2000) *Climatología de España y Portugal*, 2nd edn. Ediciones Universidad de Salamanca, Spain, pp 422
- González-Hidalgo JC, De-Luis M, Raventos J, Sanchez JR (2001) Spatial distribution of seasonal rainfall trends in a western Mediterranean area. *Int J Climatol* 21: 843–860
- González-Rouco JF, Heyen H, Zorita E, Valero F (2000) Agreement between observed rainfall trends and climate change simulations in the southwest of Europe. *J Clim* 13: 3057–3065
- González-Rouco JF, Jimenez JL, Quesada V, Valero F (2001) Quality control of monthly precipitation data in the Southwest of Europe. *J Clim* 14: 964–978
- Goodess CM, Palutikof JP (1998) Development of daily rainfall scenarios for southeast Spain using a circulation-type approach to downscaling. *Int J Climatol* 18: 1051–1083
- Goossens C, Berger A (1986) Annual and seasonal climatic variations over the Northern Hemisphere and Europe during the last century. *Ann Geophys* 4: 385–400
- Heyen H, Zorita E, von Storch H (1996) Statistical downscaling of monthly mean North Atlantic air-pressure to sea level anomalies in the Baltic Sea. *Tellus* 48A: 312–323
- Hu Q (1997) On the uniqueness of the singular value decomposition in meteorological applications. *J Clim* 10: 1762–1766
- IPCC policy makers (2001) Summary for policy makers. In: Albritton DL et al. (eds) *A report of Working Group I of the Intergovernmental Panel on Climate Change*. Geneva, Switzerland, pp 98
- IPCC technical summary (2001) Technical summary. *Climate change 2001: impacts, adaptation and vulnerability*. In: McCarthy JJ, Canziani OF, Leary NA, Dokken DJ, White KS (eds) *A Report of Working Group II of the Intergovernmental Panel on Climate Change*. Cambridge University Press, UK, pp 1000
- Janowiak JE, Gruber A, Kondragunta CR, Livezey RE, Huffman GJ (1998) A comparison of the NCEP-NCAR reanalysis precipitation and the GPCP rain gauge-satellite combined dataset with observational error considerations. *J Clim* 11: 2960–2979
- Jenkins GM, Watts DG (1968) *Spectral analysis and its applications*. Holden-Day, pp 525

- Kalnay E, Kanamitsu M, Kistler R, Collins D, Deaven D, Gandin L, Iredell M, Saha S, White G, Woolen J, Zhu Y, Chelliah M, Ebisuzaki W, Higgins W, Janowiak J, Mo KC, Kopelewski C, Wang J, Leetmaa A, Reynolds R, Jeene R, Joseph D (1996) The NCEP/NCAR 40-year Reanalysis Project. *Bull Am Meteorol Soc* 77: 437–471
- Lana X, Burgeño A (1998) Spatial characterization of annual extreme droughts in Catalonia (northeast Spain). *Int J Climatol* 18: 93–110
- Linés A (1970) The climate of the Iberian Peninsula. In: Wallén CC (ed) *World survey of climatology, volume 5: climates of Northern and western Europe*. Elsevier, Amsterdam, pp 195–239
- Lorenz E (1956) Empirical orthogonal functions and statistical weather prediction. *Sci Rept 1, Statistical forecasting Project, Department of Meteorol, MIT, Cambridge, Mass, USA*, pp 49
- Luna MY, Martín ML, Valero F, González-Rouco F (2001) Wintertime Iberian Peninsula precipitation variability and its relation to North Atlantic atmospheric circulation. In: Brunet M, López D (eds) *Detecting and modelling regional climate change and associated impacts*. Springer, Berlin Heidelberg New York, pp 369–376
- Maheras P (1988) Changes in precipitation conditions in the western Mediterranean over the last century. *J Climatol* 8: 179–189
- Maheras P, Kutiel H (1999) Spatial and temporal variations in the temperature regime in the Mediterranean and their relationship with circulation during the last century. *Int J Climatol* 19: 745–764
- Maheras P, Xoplaki E, Davies TD, Martin-Vide J, Bariendos M, Alcoforado MJ (1999) Warm and cold monthly anomalies across the Mediterranean and their relationship with circulation; 1860–1990. *Int J Climatol* 19: 1697–1715
- New MG, Hulme M, Jones PD (1999) Representing twentieth century space-time climate variability. Part I: development of a 1961–1990 mean monthly terrestrial climatology. *J Clim* 12: 829–856
- New MG, Hulme M, Jones PD (2000) Representing twentieth century space-time climate variability. Part II: Development of a 1901–1996 monthly terrestrial climate fields. *J Clim* 13: 2217–2238
- Peng S, Fyfe J (1996) The coupled patterns between SLP and sea surface temperature in the midlatitude North Atlantic. *J Clim* 9: 1824–1839
- Quadrelli R, Pavan V, Molteni F (2001) Wintertime variability of Mediterranean precipitation and its links with large-scale circulation anomalies. *Clim Dyn* 17: 457–466
- Rodriguez-Puebla C, Encinas AH, Nieto S, Garmendia J (1998) Spatial and temporal patterns of annual precipitation variability over the Iberian Peninsula. *Int J Climatol* 18: 299–316
- Romero R, Guijarro JA, Ramis C, Alonso S (1998) A 30-year (1964–1993) daily rainfall data base for the Spanish Mediterranean regions: first exploratory study. *Int J Climatol* 18: 541–560
- Romero R, Doswell III CA, Ramis C (2000) Mesoscale numerical study of two cases of long-lived quasi-stationary convective systems over Eastern Spain. *Mon Weather Rev* 128: 3731–3751
- Sumner EJ (1954) A study of blocking in the Atlantic-European sector of the northern hemisphere. *Q J R Meteorol Soc* 80: 402–416
- Sumner G, Homar V, Ramis C (2001) Precipitation seasonality in eastern and southern coastal Spain. *Int J Climatol* 21: 219–247
- Trenberth KE, Paolino DA (1980) Characteristic patterns of variability of SLP in the Northern Hemisphere. *Mon Weather Rev* 108: 856–872
- Trigo RM, Palutikof JP (1999) Simulation of daily temperatures for climate change scenarios over Portugal: a neural network approach. *Clim Res* 13: 45–59
- Trigo RM, Palutikof JP (2001) Precipitation scenarios over Iberia: a comparison between direct GCM output and different downscaling techniques. *J Clim* 14: 4422–4446
- Valero F, Luna MY, Martín ML (1997) An overview of a heavy rain event in southeastern Iberia: the role of large-scale meteorological conditions. *Ann Geophys* 15: 494–502
- von Storch H, Navarra A (1995) *Analysis of climate variability. Applications of statistical techniques*. Springer, Berlin Heidelberg New York, pp 334
- von Storch H, Zwiers FW (1999) *Statistical analysis in climate research*. Cambridge University Press, Cambridge, UK, pp 484
- von Storch H, Zorita E, Cubasch U (1993) Downscaling of global climate estimates to regional scales: an application to the Iberian rainfall in wintertime. *J Clim* 6: 1161–1171
- Wallace JM, Smith C, Bretherton CS (1992) Singular value decomposition of wintertime sea surface temperature and 500-mb height anomalies. *J Clim* 5: 561–576
- Wheeler DA (1989) Meteorological gatherings from Spain. *Weather* 44(1): 12–20
- Wibig J (1999) Precipitation in Europe in relation to circulation patterns at the 500 hPa level. *Int J Climatol* 19: 253–269
- Widmann M, Bretherton CS (2000) Validation of mesoscale precipitation in the NCEP reanalysis using a new grid-cell dataset for the northwestern United States. *J Clim* 13: 1936–1950
- Xoplaki E, González-Rouco JF, Gyalistras D, Luterbacher J, Rickli R, Wanner H (2003a) Interannual summer air temperature variability over Greece and its connection to the large-scale atmospheric circulation and Mediterranean SSTs 1950–1999. *Clim Dyn* 20: 537–554
- Xoplaki E, González-Rouco JF, Luterbacher J, Wanner H (2003b) Mediterranean summer air temperature variability and its connection to the large scale circulation and SSTs. *Clim Dyn* 20: 723–739
- Zorita E, Kharin V, von Storch H (1992) The atmospheric circulation and sea surface temperature in the North Atlantic area in winter: their interaction and relevance for Iberian Precipitation. *J Clim* 5: 1097–1108